Supporting Information

Dual-responsive porous ionic liquids with the reversible phase transition behaviors based on ionic liquid crystal for CO_2 and C_2H_4 adsorption

Xiaoqian Li[a], Dechao Wang[a], Zhongjie He[a], Fangfang Su[a], Jing Zhang[a], Yudeng Wang[a], Yangyang Xin[a], Hongni Wang[a], Dongdong Yao[a], Mingtao Li[b]*, and Yaping Zheng[a]**

[a] School of Chemistry and Chemical Engineering, Northwestern Polytechnical University, Xi'an 710129, P. R. China

[b] School of Chemical Engineering and Technology, Xi'an Jiaotong University, Xi'an 710049, P. R. China

*Corresponding Author:

E-mail: yaodd@nwpu.edu.cn (Dongdong. Yao);

lmt0558@mail.xjtu.edu.cn (Mingtao. Li);

zhengyp@nwpu.edu.cn (Yaping. Zheng).

Contents

1. General synthesis

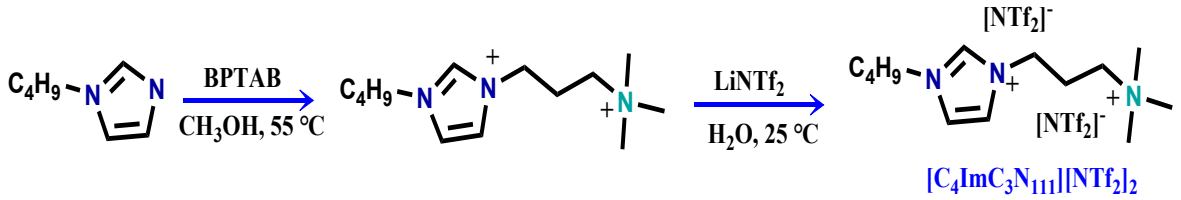

Scheme. S1 Synthetic routes of ILCs asymmetry $[C_4ImC_3N_{111}][NTf_2]_2$.

1.1. Synthesis of ZIF-8

ZIF-8 nanocrystals were synthesized based on previous studies. [1, 2] $Zn(NO_3)_2 \cdot 6H_2O$ (5.9 g, 20 mmol) was dissolved in 20mL of methanol. Then, the solution was added to another solution consisting of 2-methylimidazole (6.56 g, 80 mmol) in 180mL of methanol stirring for 1 h at 50 °C. The precipitate was separated from the colloidal dispersion by centrifugation (8000 rpm, 8 mins) and washed with methanol six times. The product was dried at 80 °C in a vacuum oven overnight.

1.2. Synthesis of ZIF-67

ZIF-67 nanocrystals were synthesized according to the previous reports.[3-5] $Co(NO_3)_2 \cdot 6H_2O$ (8.0 g, 27.5 mmol) and 2-methylimidazole (7.10, 86.9 mmol) were dissolved methanol (100 mL), respectively. Then the solution of 2-methylimidazole was added to the methanol solution of $Co(NO_3)_2$. The reaction mixture was stirred for 24 h under 30 °C at 600 rpm. The solid product was collected by centrifuging the reaction mixture at 8000 rpm. The product was purified by washing with methanol and centrifuging three times at 8000 rpm for 8 min, then was dried at 80 °C in a vacuum oven overnight.

1.3. Synthesis of UIO-66-NH_2

UiO-66-NH_2 was synthesized by dissolving $ZrCl_4$ (240 mg, 1.03 mmol) and 2-aminoterephthalic acid (NH_2-BDC, 186 mg, 1.03 mmol) in 60 mL of DMF. After mixing, acetic acid (3.53 mL) was added. The mixture was heated in a microwave synthesizer at 120 °C for 4 h, and the radiation power was 800 W. After cooling to room temperature, the product was collected by centrifugation and washed by fresh DMF and methanol three times each.

2. Characterization of $[C_4ImC_3N_{111}][NTf_2]_2$

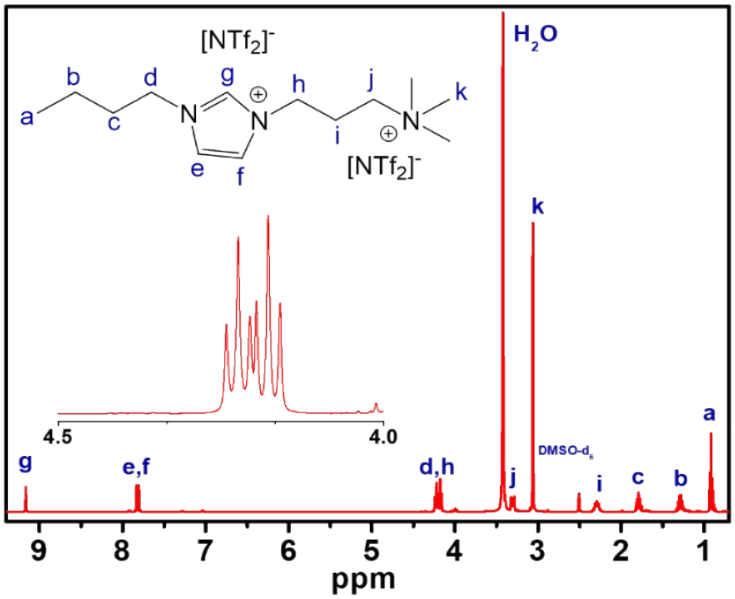

Fig. S1 ^{1}H NMR (298K, 400 MHz, DMSO-d_6) spectroscopes of $[C_4ImC_3N_{111}][NTf_2]_2$.
^{1}H NMR (400 MHz, DMSO-d_6, δ): 9.16 (s, 1H), 7.82 (dt, 2H), 4.20 (dt, 4H), 3.06 (s, 9H), 2.29 (s, 2H), 1.86-1.74 (m, 2H), 1.35-1.23 (m, 2H), 0.92 (t, 3H).

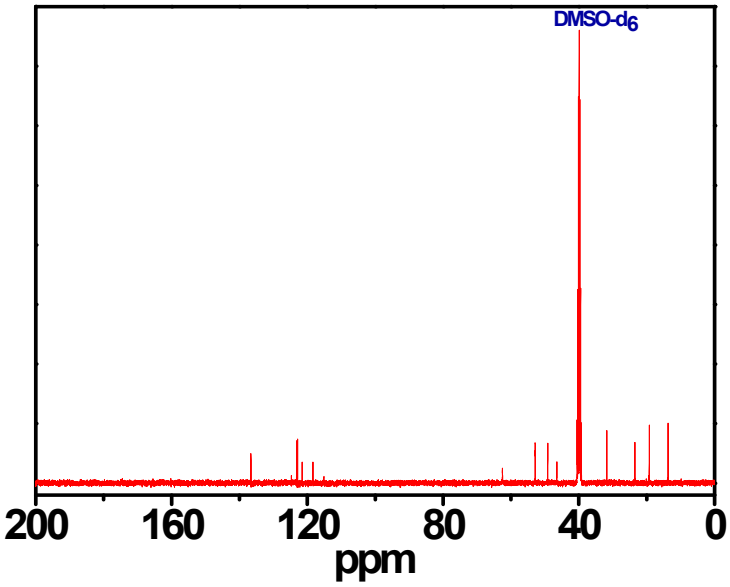

Fig. S2 ^{13}C NMR (298K, 400 MHz, DMSO-d_6) spectroscopy of $[C_4ImC_3N_{111}][NTf_2]_2$.

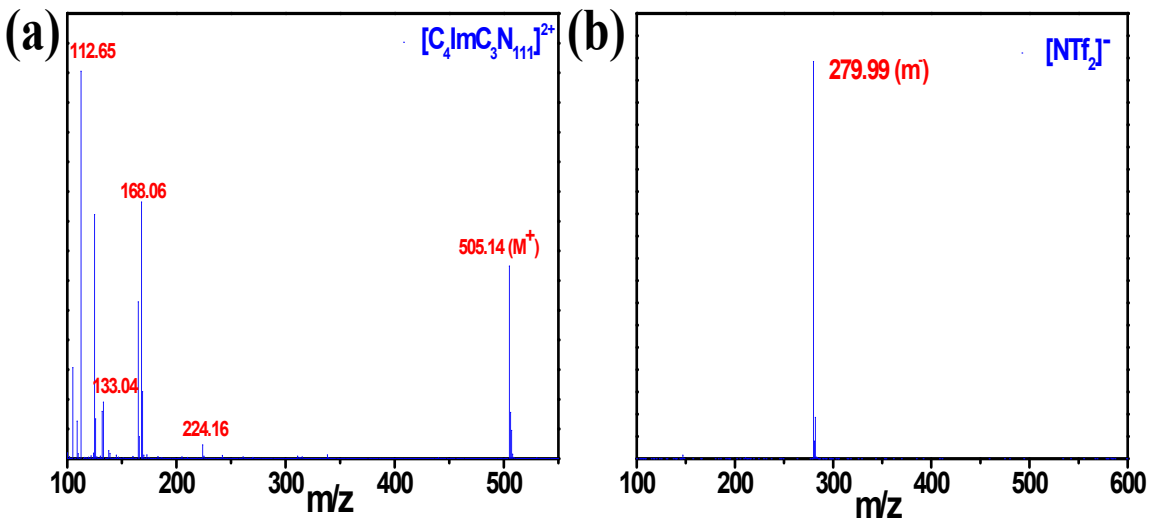

Fig. S3 ESI-MS spectroscopes of $[C_4ImC_3N_{111}][NTf_2]_2$ in ESI positive (a) and ESI negative (b), respectively. MS (ESI positive) m/z(%): $[C_4ImC_3N_{111}][NTf_2]^+$: calcd: 505.00 g·mol^{-1}; found: 505.14 g·mol^{-1}. And, MS (ESI negative) $[NTf_2]^-$ m/z(%): calcd: 279.99 g·mol^{-1}; found: 279.92 g·mol^{-1}.

3. Characterization of SRPILs

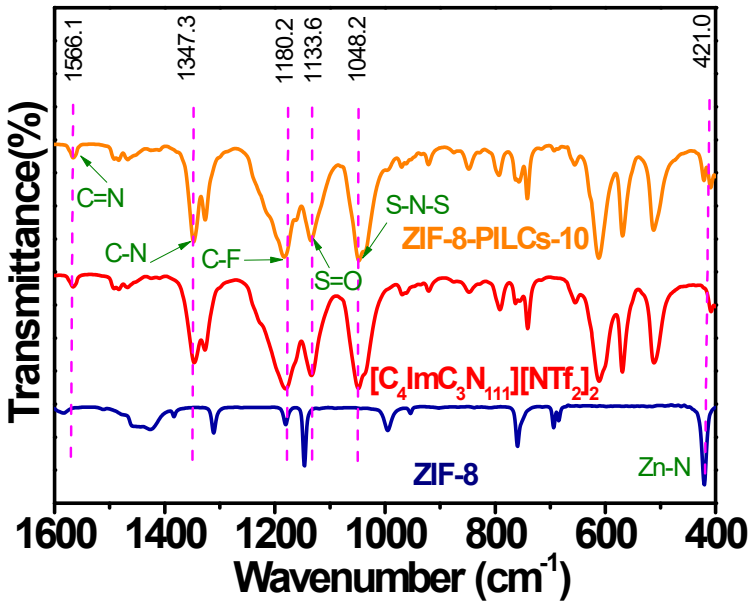

Fig. S4 FT IR spectra of ZIF-8, $[C_4ImC_3N_{111}][NTf_2]_2$ and ZIF-8-PILCs-10, respectively.

Characteristic peaks of ILCs at 1180.3 cm^{-1}, 1133.7 cm^{-1}, 1048.2 cm^{-1} can be assigned to the $\nu_{as}(CF_3)$, $\nu_s(S=O)$ and $\nu_{as}(S-N-S)$ in the $[TNf_2]^-$ anion. And, the bands at 3152.64 cm^{-1}, 1566.17 cm^{-1} and 1347.39 cm^{-1} corresponded to the ν_{as} (C=C), ν(C=N) and ν(C-N) in the $[C_4ImC_3N_{111}]^{2+}$cation, respectively. A small blue shift towards higher energy is observed in the ZIF-8-SRPILs, indicating that the $[TNf_2]^-$ anion and $[C_4ImC_3N_{111}]^{2+}$ cation interactions are affected by ZIF-8.

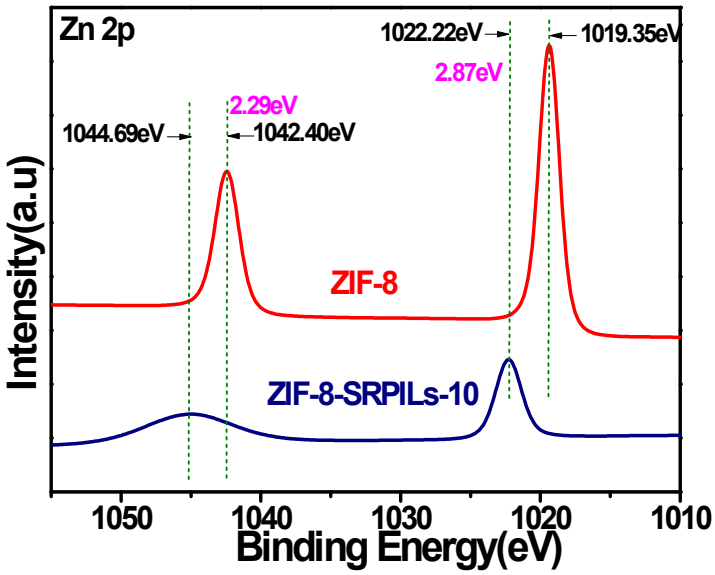

Fig. S5. High-resolution Zn 2p XPS spectra of ZIF-8 and ZIF-8-SRPILs, respectively.

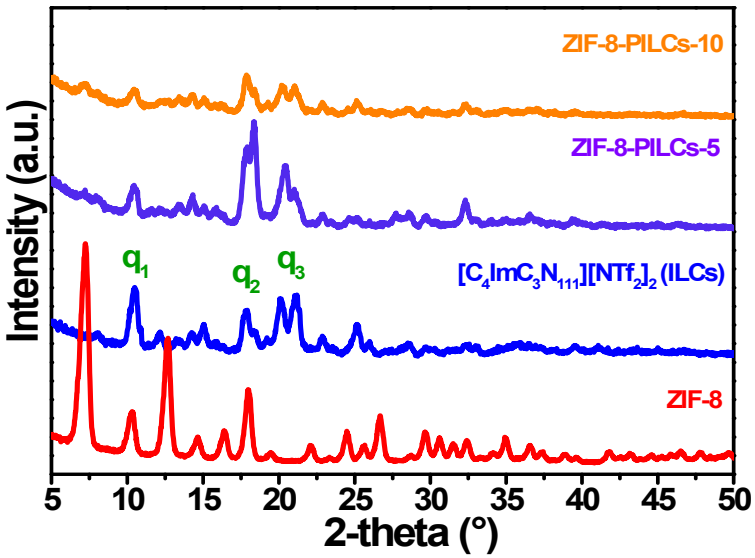

Fig. S6 PXRD patterns for ZIF-8, $[C_4ImC_3N_{111}][NTf_2]_2$, ZIF-8-PILC-5, and ZIF-8-PILC-10 after shearing stimulation.

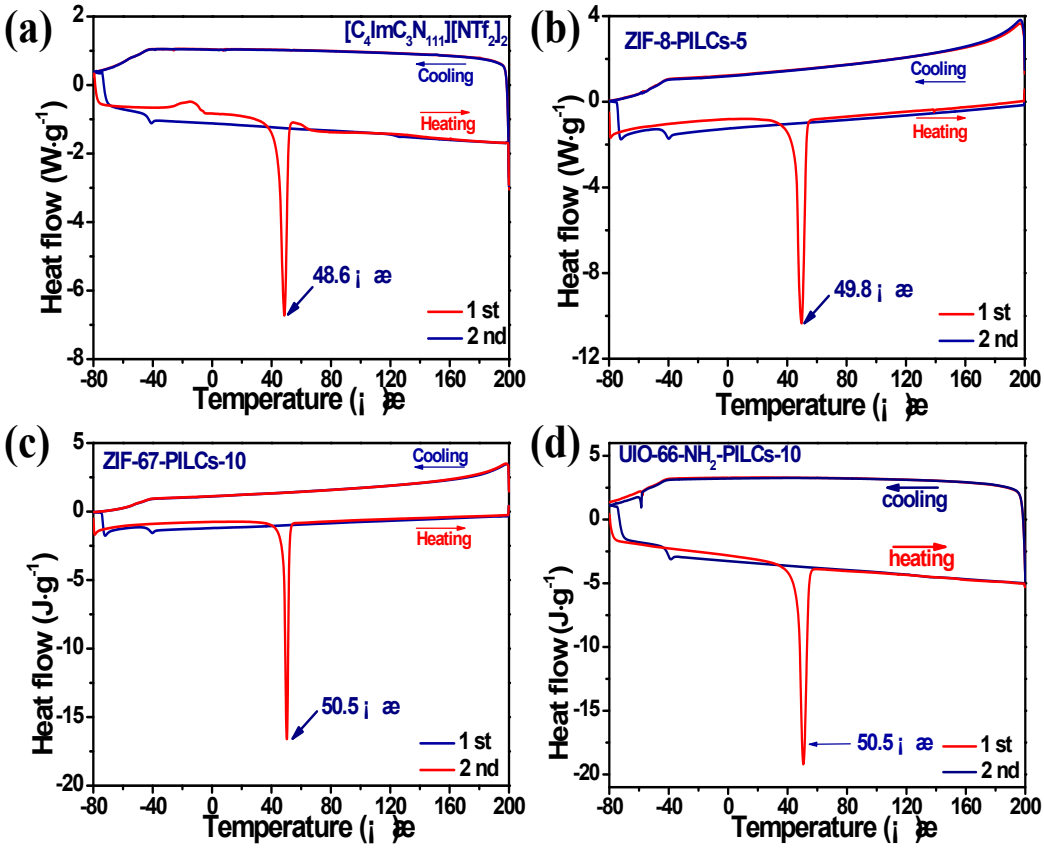

Fig. S7 DSC traces of $[C_4ImC_3N_{111}][NTf_2]_2$, ZIF-8-PILCs-5, ZIF-67-PILCs-10, and UIO-66-NH_2-PILCs-10, under N_2 atmosphere at a rate of 10 °C·min^{-1}.

Table S1 Transition temperatures and the corresponding enthalpies of ILCs, and PILCs obtained *via* DSC traces (Cr: crystalline phase, LCs: liquid crystals, Col_r: columnar phase, and Iso: isotropic phase).

Samples	**Phase transition behaviors**					
	First heating			Second heating		
	Transition	T_{rev} (°C)	ΔH_{regen} (W·g^{-1})	Transition	T_{rev}(°C)	ΔH_{regen} (W·g^{-1})
$[C_4ImC_3N_{111}][NTf_2]_2$	Cr-Col	-14.1	20.8	Cr-Col	-75.1	7.6
	Col-Iso	48.6	175.01	Col-Iso	-40.8	5.3
ZIF-8-PILCs-10	Cr-Col	-78.8	60.7	Cr-Col	-71.8	60.7
	Col-Iso	49.86	324.9	Col-Iso	-39.5	8.0
ZIF-67-PILCs-10	Cr-Col	-77.8	42.7	Cr- Col	-71.3	31.1
	Col-Iso	48.8	334.1	Co-Iso	-39.5	6.7

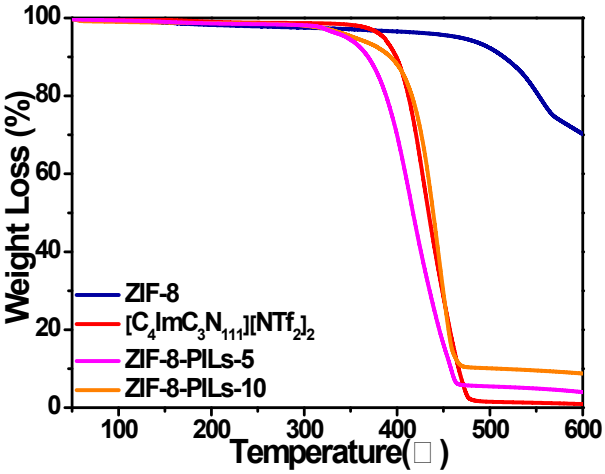

Fig. S8 TGA curves of ZIF-8, $[C_4ImC_3N_{111}][NTf_2]_2$, 5 wt% and 10 wt% ZIF-8 dispersions in ILCs, respectively.

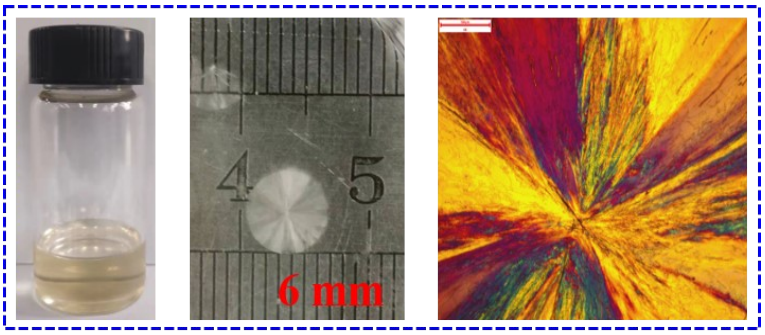

Fig. S9 Photograph of the $[C_4ImC_3N_{111}][NTf_2]_2$, the crystal of $[C_4ImC_3N_{111}][NTf_2]_2$, which are taken out into a glass Petri dishes and the correspond of POM image at 25 °C.

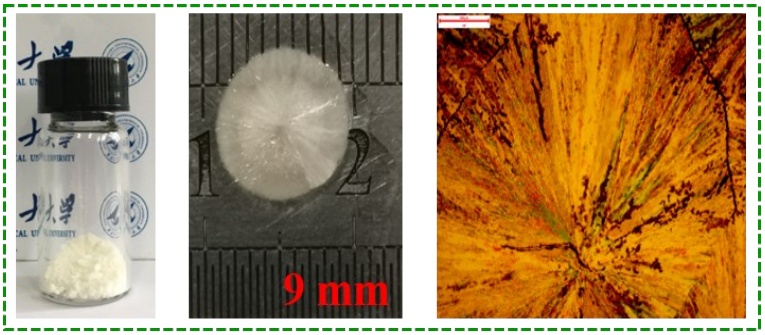

Fig. S10 Photograph of the ZIF-8-PILCs-10, the crystal of PILCs which are taken out into a glass Petri dishes and the correspond of POM image at 25 °C.

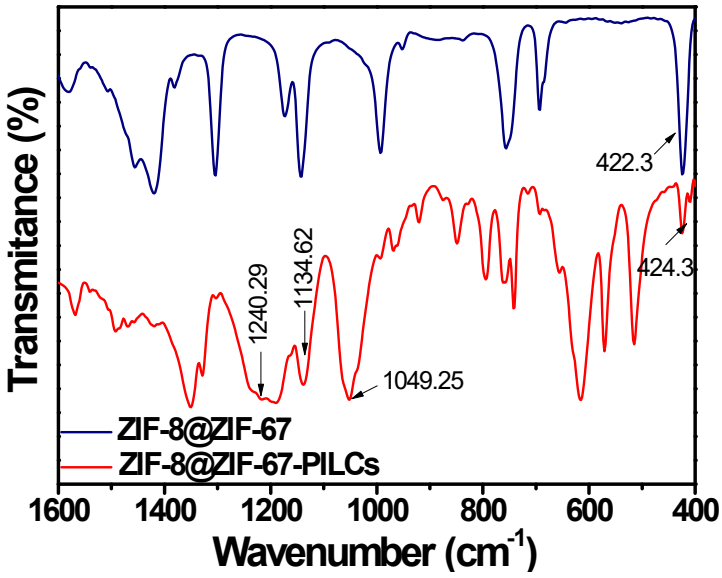

Fig. S11 FT IR spectra of ZIF-8@ZIF-67, and ZIF-8@ZIF-67-PILCs, respectively.

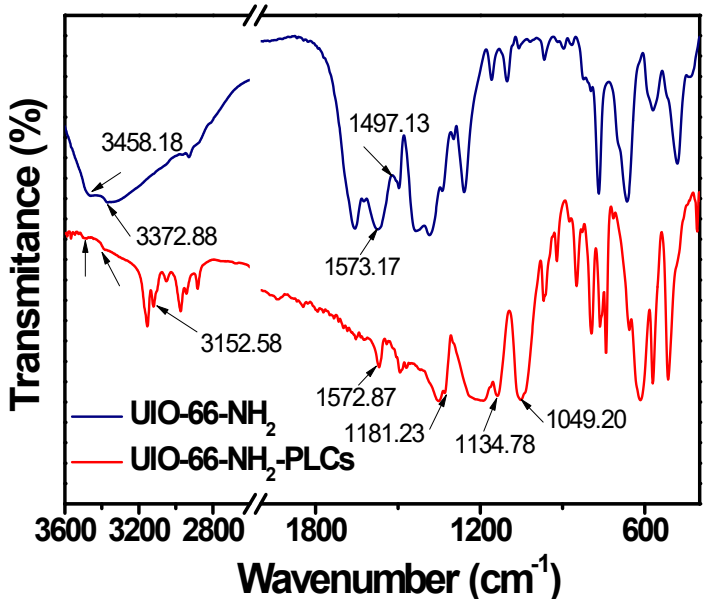

Fig. S12 FT IR spectra of UIO-66-NH_2, and UIO-66-NH_2-PILCs-10, respectively.

The absorption bands at 3458.18 and 3372.88 cm^{-1} were corresponding to symmetric and asymmetric vibrations of -NH_2 groups on the organic linker. The absorption band at 1573.17 cm^{-1} revealed the possibility of reaction of Zr^{4+} with -COOH. The absorption band at 1497.13 cm^{-1} originated from the aromatic structure. Besides, peaks at 1181.23 cm^{-1} (-CF_3), 1134.78 cm^{-1} (S-N-S), 1049.20 cm^{-1} (S=O) were observed in the UIO-66-NH_2-PILCs, indicates that UiO-66-NH_2 was successfully coated with ILCs.

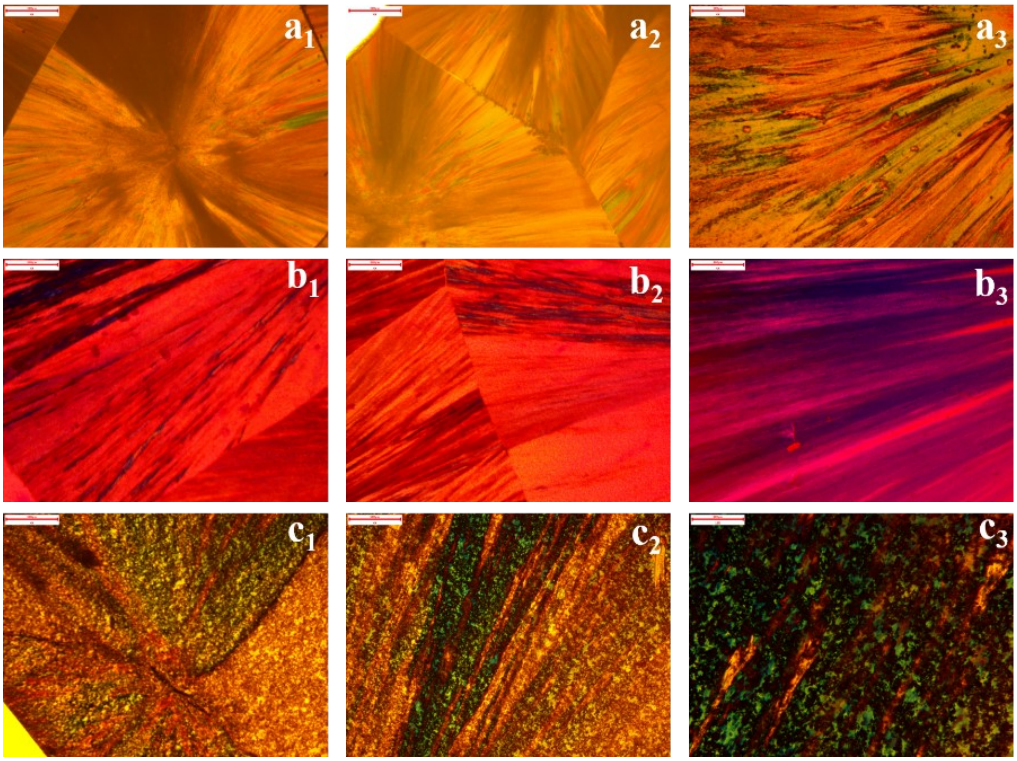

Fig. S13 Polarizing optical micrographs (POM) of ZIF-8@ZIF-67-PILCs-5 ($a_{1\text{-}3}$), ZIF-67-PILCs-5 ($b_{1\text{-}3}$), UIO-66-NH_2-PILCs-5 ($c_{1\text{-}3}$), respectively.

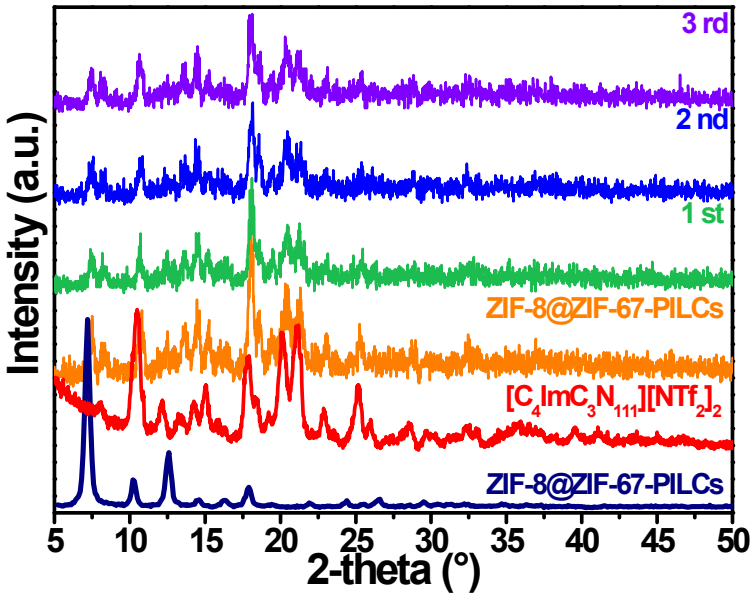

Fig. S14 PXRD patterns of ILCs for ZIF-8@ZIF-67, $[C_4ImC_3N_{111}][NTf_2]_2$, and ZIF-8@ZIF-67-PILCs and corresponding three cycles, respectively.

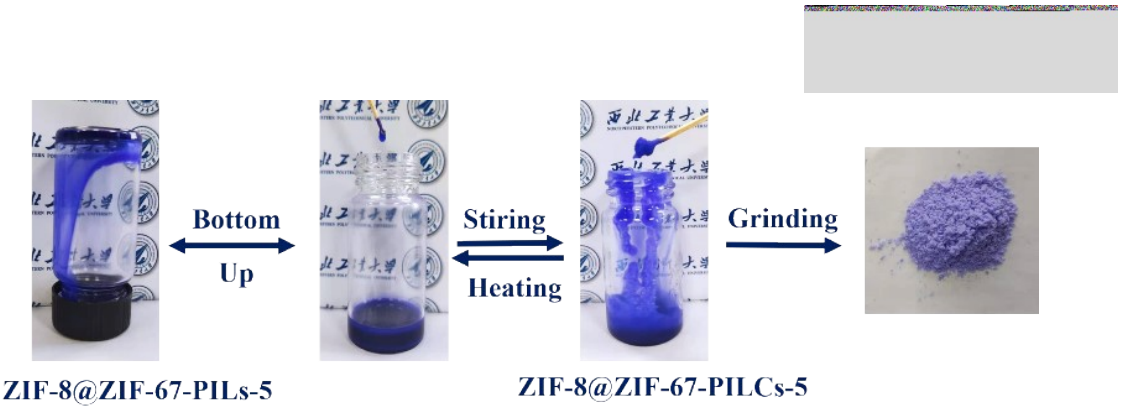

Fig. S15 Photographs of ZIF-8@ZIF-67-SRPILs showed reversible transition behaviors of PLs and PILCs induced by heating and shearing.

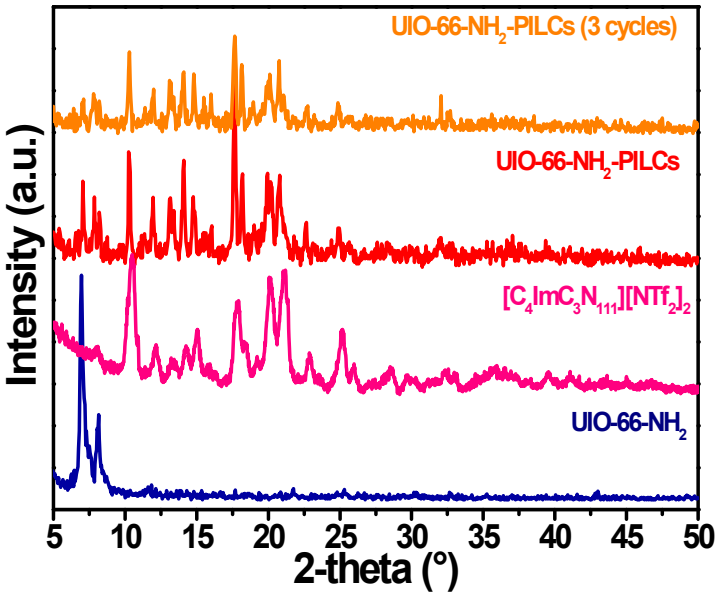

Fig. S16 PXRD patterns of ILCs for UIO-66-NH_2, $[C_4ImC_3N_{111}][NTf_2]_2$, UIO-66-$NH_2$-PILCs, and corresponding three cycles, respectively.

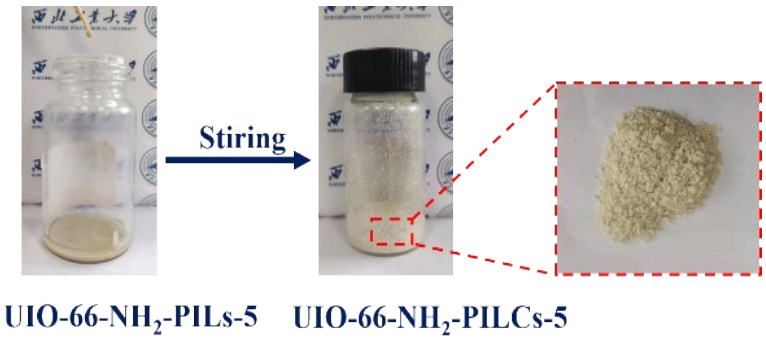

Fig. S17 Photographs of UIO-66-NH_2-SRPILs transform to UIO-66-NH_2-PILCs induced by shearing.

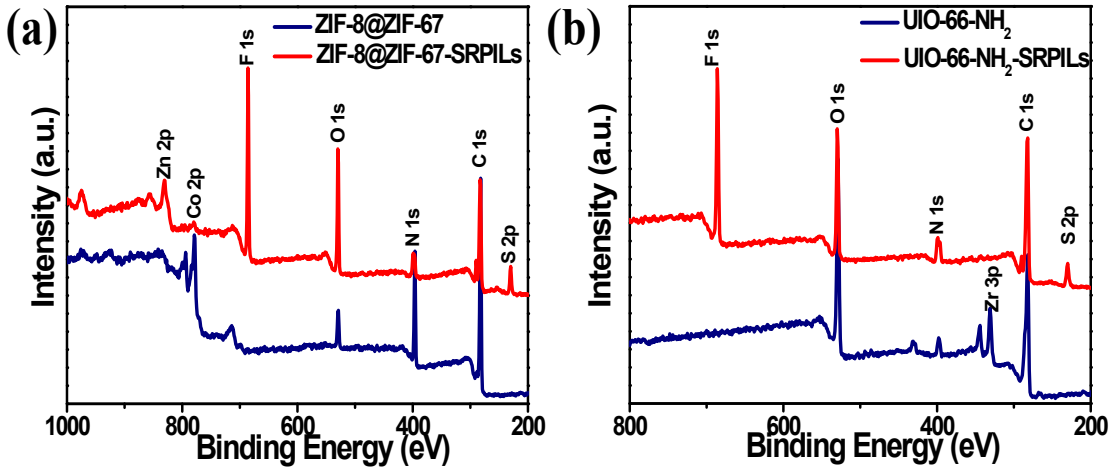

Fig. S18 The wide scan spectrum of ZIF-8@ZIF-67, ZIF-8@ZIF-67-SRPILs (a), and UIO-66-NH_2, UIO-66-NH_2-SRPILs, respectively.

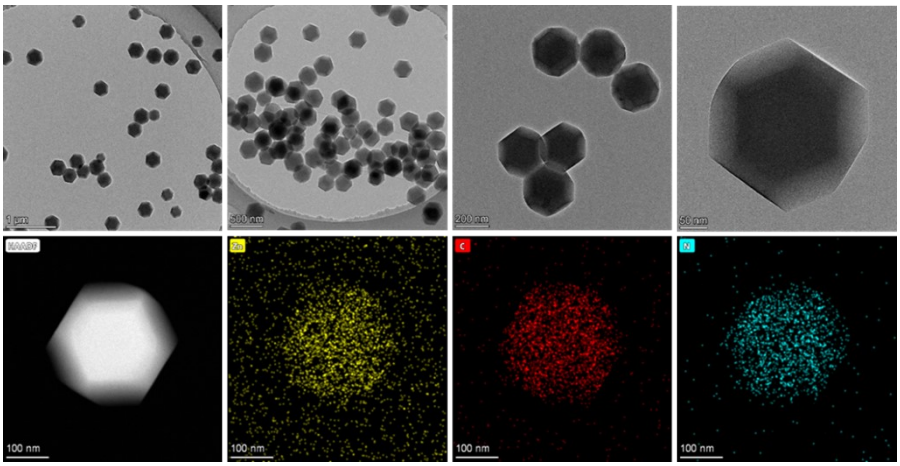

Fig. S19 TEM images of ZIF-8 and corresponding elemental mapping images of Zn, C, N, respectively.

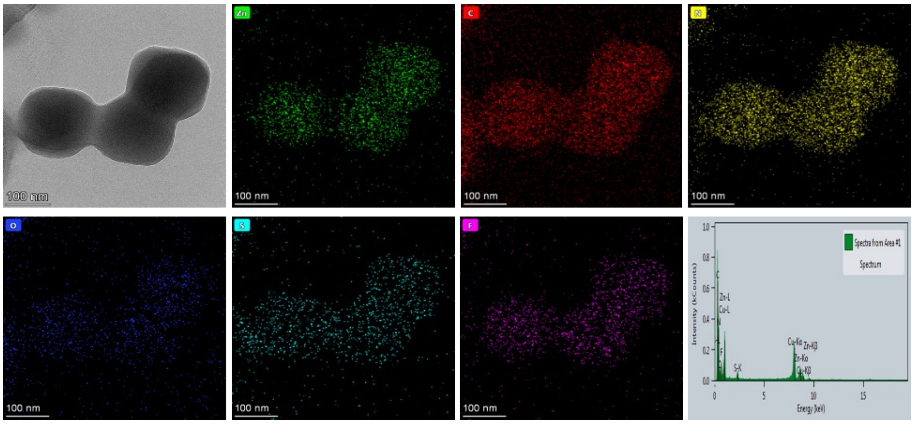

Fig. S20 TEM images of ZIF-8-SRPILs-5 and corresponding elemental mapping images of C, N, O, F, S, respectively.

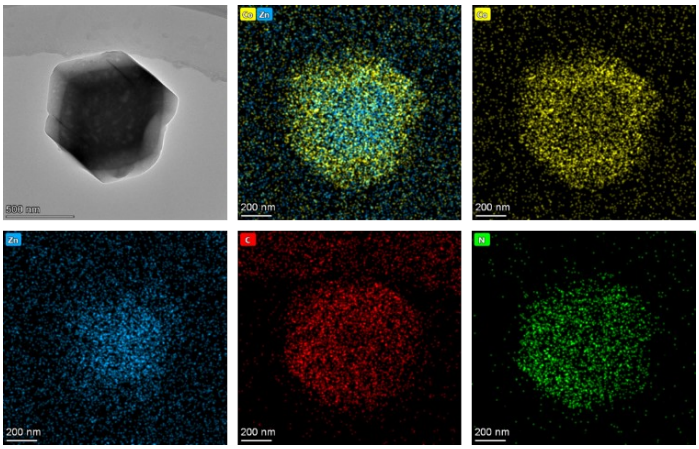

Fig. S21 TEM images of ZIF-8@ZIF-67 and corresponding elemental mapping images of Co, Zn, C, N, respectively.

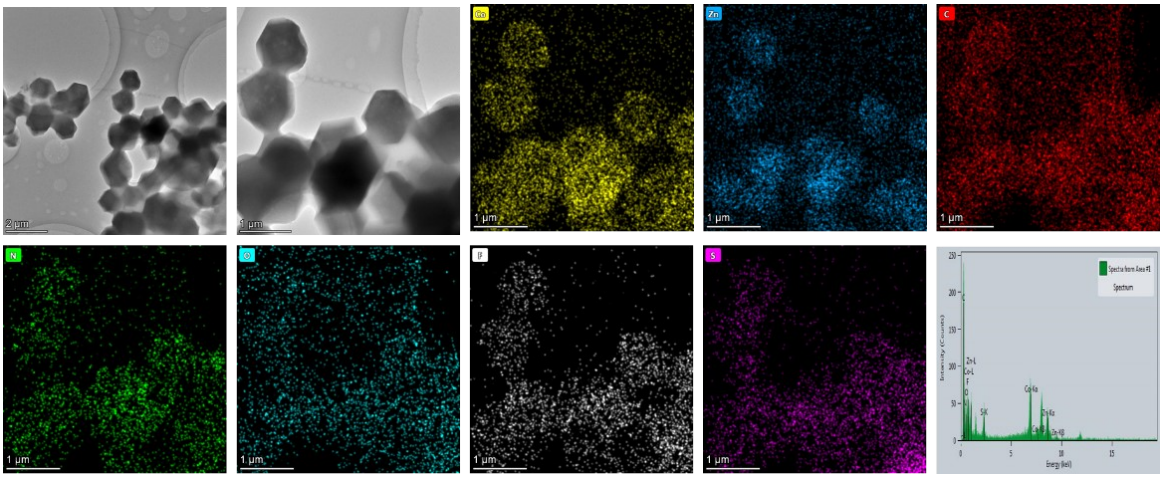

Fig. S22 TEM images of ZIF-8@ZIF-67-SRPILs-5 and corresponding elemental mapping images of Co, Zn, C, N, O, F, S, respectively.

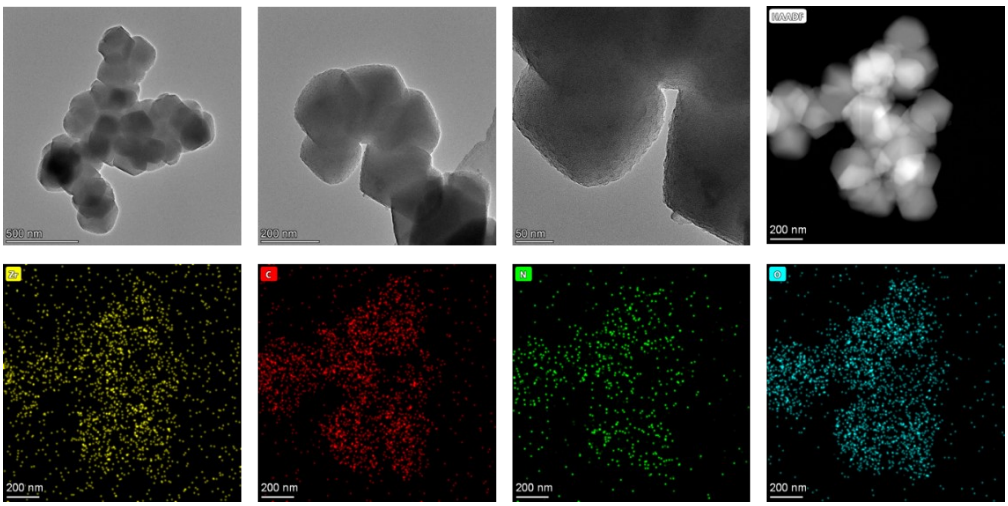

Fig. S23 TEM images of UIO-66-NH_2 and corresponding elemental mapping images of Zr, C, N, O, respectively.

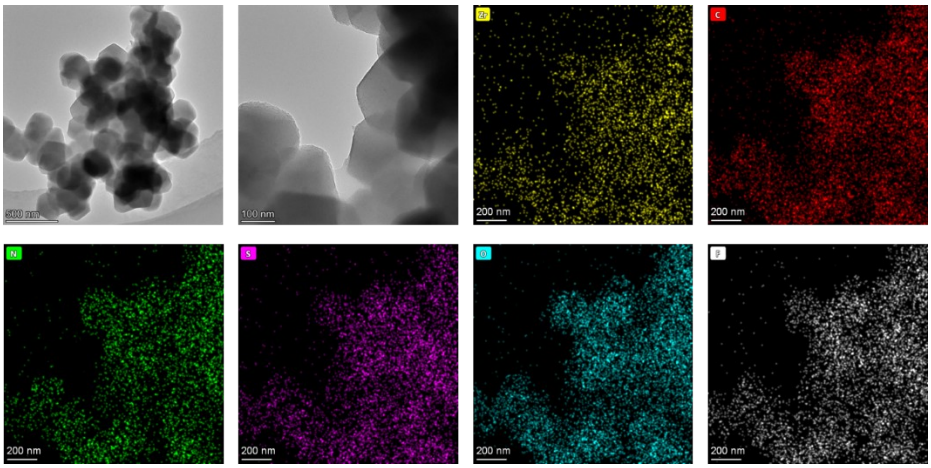

Fig. S24 TEM images of UIO-66-NH_2-SRPILs-5 and corresponding elemental mapping images of C, N, O, F, S, respectively.

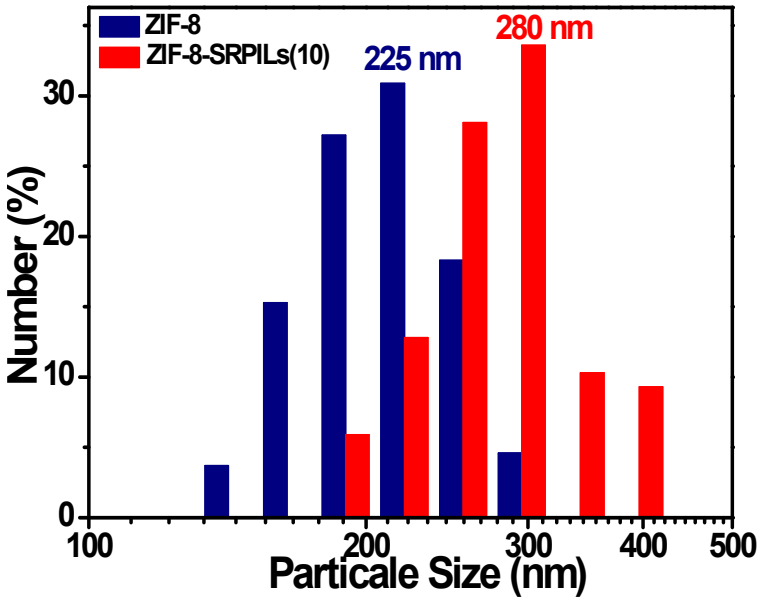

Fig. S25 Dynamic light scattering (DLS) analysis of ZIF-8 and ZIF-8-SRPILs-10 in ethanol, respectively.

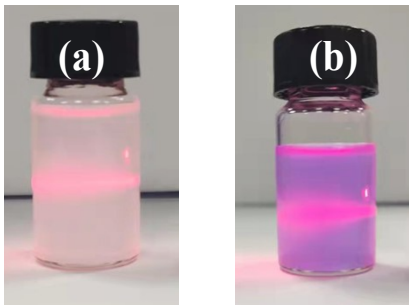

Fig. S26 Tyndall effect of ZIF-8-SRPILs, ZIF-8@ZIF-67-SRPILs after exposed to air for more 360 days. PILs (40 mg) dispersions in CH_3OH solvents (5 mL) for 2h, respectively.

Tables S2. The pore structure properties of ZIF-8, ZIF-67, ZIF-8@ZIF-67, and UIO-66-NH_2, respectively.

Samples	Properties			
	S_{BET}[a] (m^2/g)	S_L[b] (m^2/g)	V_t[c] (cm^3/g)	D_{H-K}[d] (nm)
ZIF-8	1308.68	1912.87	0.9595	0.7801
ZIF-67	1298.21	1932.92	0.7026	0.6788
ZIF-8@ZIF-67	1129.26	1605.01	1.0163	0.5527
UIO-66-NH_2	924.05	1048.65	0.4580	0.8635
ZIF-8-PILs-5	1.08	-	-	-

[a] Surface area calculated from the BET equation in the relative pressure range of 0.04-0.32. [b] Surface area calculated using the Langmuir method. [c] Total pore volume calculated in the relative pressure P/P0=0.9967. [d] The average pore diameter was calculated by using the H-K(original) method.

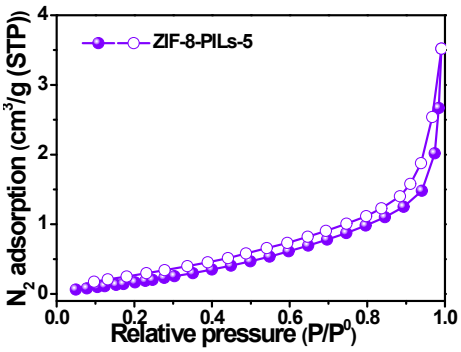

Fig. 27 N_2 adsorption-desorption isotherms of ZIF-8-PILs-5 at 77 K.

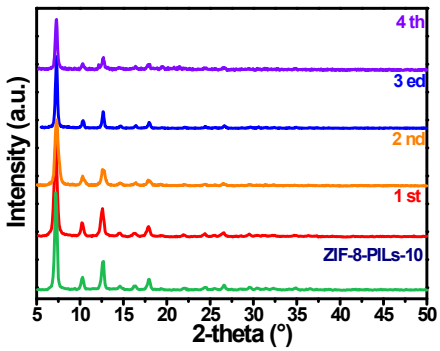

Fig. S28 PXRD patterns of ZIF-8-SRPLs-10 for 4 times reversibly phase transitions cycles *via* mechanical stimuli and heating, respectively.

Table. S3 Compare SRPILs with PLs in previously reported.

Type	Sample name	Viscosity（mPa·s /at 25℃）	CO_2 adsorption (25 ℃)	References
I	HS@OS@PEGs	6800 at 40℃	CO_2/N_2 separation	6
		4200 at 50℃		
	HCS-liquids	High viscosity	CO_2/N_2 separation	7
	PS-OS@SiNRs	Like-gel	3.3, 4.8 wt% (0 ℃)	8
	UiO-66-liquids	14000	0.25 mmol·g^{-1}（10 bar 25 ℃）	9
	UiO-66-KH550-PDMS400	1100	23 mL/g (10 bar)	10
	UiO-66-SID-PDMS400	1500	34 mL/g (10 bar)	
	HCS-PILs-PEGS	8900 at 50℃	1.8 mmol·g^{-1} (3 bar)	11
II	Crown-ether cage @15-crown-5	20	CH_4 adsorption	12
	3^3:13^3_{DCBC}	14.93±0.038	CH_4 and Xenon uptake	13
	3^3:13^3_{TBA}	32.46±0.53		
	3^3:13^3_{MS}	9.84±0.00057		
	3^3:13^3_{DCT}	3.70±0.0031		
	3^3:13^3_{HAP}	9.82±0.015		
III	H-ZSM-5-liquid/[P66614][Br]	9550	2 wt% (10 bar)	14
	PL1	5100	30.8 cm^3/g (10 bar)	15
	PL4	6000	29.0 cm^3/g (10 bar)	
	PL5	11000	12.4 cm^3/g (10 bar)	
	ZIF-67-PLs-2	543.4	5.77 mmol·g^{-1} (1bar)	16
	ZIF-67-PLs-5	938.0	7.12 mmol·g^{-1} (1bar)	
	ZIF-67-PLs-10	1896.7	9.54 mmol·g^{-1} (1bar)	
	ZIF-8(200nm)-PLs-5	900.5	-	
	ZIF-8(500nm)-PLs-5	832.5	-	
	PLs1(1000)-5%	49	1.30 cm^3/g (1 bar)	17
	PLs2(1000)-5%	59	1.06 cm^3/g (1 bar)	
	ZIF-8-*g*-BPEI PLs	1700	0.98 mL/g (10 bar)	18

4. Supporting Information of Video

Video 1. ZIF-8-PILCs-10 with sticky liquids.

Video 2. Stimuli-responsive of ZIF-8-PILCs-10 by a shear-induced liquid phase transition to the solid phase.

Video 3. Stimuli-responsive of ZIF-8@ZIF-67-PILCs-5 by a shear-induced phase transition.

5. Reference

1. S. Tanaka, K. Kida, M. Okita, Y. Ito, Y. Miyake, *Chem. Lett*, 2012, **41**, 1337-1339.
2. Y. Ban, Z. Li, Y. Li, Y. Peng, H. Jin, W. Jiao, A. Guo, P. Wang, Q. Yang, C. Zhong, W. Yang, *Angew Chem Int Ed Engl*, 2015, **54**, 15483-15487.
3. S. Ghoshal, S. Zaccarine, G. C. Anderson, M. B. Martinez, K. E. Hurst, S. Pylypenko, B. S. Pivovar, S. M. Alia, *ACS Appl. Energy Mater*, 2019, **2**, 5568-5576.
4. G. Zhong, D. Liu, J. Zhang, *J. Mater. Chem. A*, 2018, **6**, 1887-1899.
5. S. Li, S. Peng, L. Huang, X. Cui, A. M. Al-Enizi, G. Zheng, *ACS Appl. Mater. Interfaces*, 2016, **8**, 20534-20539.
6. J. C. Zhang, S. H. Qiao, Z. A. Mahurin, S. M. Chen, J. Fang, Y. Wan, S. Nelson, K. Zhang, P. Dai, S., *Angew Chem Int Ed Engl*, 2015, **54**, 932-936.
7. J. A. S. P. Li, J. Zhang, Shannon M. Mahurin, Y. Sheng, Z. Qiao, X. Hu, G. Cui, D. Yao, Suree Brown, Y. Zheng, S. Dai, *Angew. Chem*, 2017, **129**, 15154-15158.
8. R. Kumar, P. Dhasaiyan, P. M. Naveenkumar, K. P. Sharma, *Nanoscale Adv*, 2019, **1**, 4067-4075.
9. D. Wang, Y. Xin, X. Li, H. Ning, Y. Wang, D. Yao, Y. Zheng, Z. Meng, Z. Yang, Y. Pan, P. Li, H. Wang, Z. He, W. Fan, *ACS Appl. Mater. Interfaces*, 2021, **13**, 2600-2609.
10. Y. Xin, D. Wang, D. Yao, H. Ning, X. Li, X. Ju, Y. Zhang, Z. Yang, Y. Xu, Y. Zheng, *N. J. Chem*, 2022, **46**, 2189-2197.
11. F. Su , X. Li. Y. Wang , Z. He , L. Fan , H. Wang , J. Xie , Y. Zheng , D. Yao *Sep. Purif. Technol*, 2021, **277**, 119410-119419.
12. N. Giri, M. G. Del Popolo, G. Melaugh, R. L. Greenaway, K. Ratzke, T. Koschine, L. Pison, M. F. Gomes, A. I. Cooper, S. L. James, *Nat*, 2015, **527**, 216-220.
13. R. J. Kearsey, B. M. Alston, M. E. Briggs, R. L. Greenaway, A. I. Cooper, *Chem. Sci*, 2019, **10**, 9454-9465.
14. P. Li, H. Chen, J. A. Schott, B. Li, Y. Zheng, S. M. Mahurin, D. E. Jiang, G. Cui, X. Hu, Y. Wang, L. Li, S. Dai, *Nanoscale*, 2019, **11**, 1515-1519.
15. S. He, L. Chen, J. Cui, B. Yuan, H. Wang, F. Wang, Y. Yu, Y. Lee, T. Li, *J. Am. Chem. Soc*, 2019, **141**, 19708-19714.
16. X. Li, D. Wang, Z. He, F. Su, N. Zhang, Y. Xin, H. Wang, X. Tian, Y. Zheng, D. Yao, M. Li, *Chem. Eng. J*, 2021, **417**, 129239.
17. X. Li, D. Wang, Z. He, X. Tian, Y. Xin, F. Su, H. Wang, J. Zhang, X. Li, M. Li , Y. Zheng, *Chem. Eng. J*, 2022, **429**, 132296-132204.
18. X. Li, D. Wang, H. Ning, Y. Xin, Z. He, F. Su, Y. Wang, J. Zhang, H. Wang, L. Qian, Y. Zheng, D. Yao, M. Li, *Sep. Purif. Technol,* 2021, **276**, 119305-119314.